THE JOURNAL OF PHYSICAL CHEMISTRY C
A JOURNAL OF THE AMERICAN CHEMICAL SOCIETY

pubs.acs.org/JPCC

Perspective

Toward Understanding and Controlling Organic Reactions on Metal Oxide Catalysts

Victor Fung,* Michael Janik,* Steven Crossley,* Ya-Huei Cathy Chin,* and Aditya Savara*

Cite This: *J. Phys. Chem. C* 2023, 127, 13451−13465

Read Online

ACCESS | Metrics & More | Article Recommendations

ABSTRACT: Metal oxides have structurally complex surfaces on which a variety of adsorption site types can occur, including cation sites, anion sites, oxygen vacancy sites, and Brønsted acid sites. These sites can catalyze the catalytic transformation of organic molecules via diverse routes, thus enabling H abstraction, O abstraction, C−C bond formation, and other reactions. This Perspective provides an update on recent advances and future directions for various organic reactions on metal oxide catalyst surfaces, particularly for C−H activation of alkanes and for C−C bond formation with organic oxygenate reactants. We put emphasis on the molecular scale details, on the active site structures required to enable the formation of kinetically relevant transition states, energetic descriptors, as well as contemporary ideas to enable low activation energies. This progress has been enabled by specialized experiments and the increased capabilities of modern electronic structure calculations.

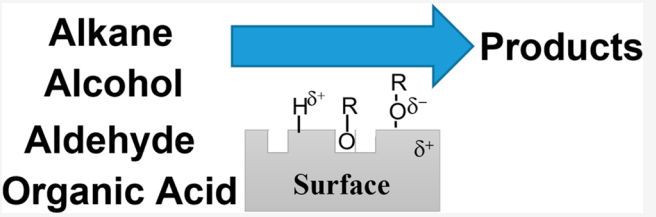

INTRODUCTION

Reactions of organic molecules on metal oxide surfaces have been well studied, though open questions remain.[1−18] Recently, there has been increased research on conversion of methane as well as organic oxygenates over metal oxide surfaces. This Perspective provides an update on recent advances in organic reactions on metal oxide catalysts and future directions, with emphasis on the active site structures required to enable the formation of kinetically relevant transition states as well as contemporary ideas to enable low activation energies. Some of the ways that transition states can be altered during organic transformations on metal that oxides are included are (a) by electronic modulation of the adsorption site, (b) by introducing oxygen vacancy sites, (c) by interactions of adsorbed intermediates with neighboring species, and (d) by confinement effects in pores. The site ensembles that are present on metal oxides and similar materials (such as Lewis acids adjacent to Lewis bases) can enable unique selectivities and activities, as well as tunability through elemental substitution and other methods.

The catalytic reactions that will be covered are not all new but are being increasingly understood or controlled at the atomistic scale, with explicit electronic structure calculations of plausible states playing a significant role in understanding the complexity of local sites and geometries. In a rough sense, this Perspective will move from the electronic structure scale toward the reaction network scale, with case examples grouped by reaction type.

ELECTRONIC STRUCTURE CONSIDERATIONS AND DESCRIPTORS

The first step in catalytic conversion of a molecule is adsorption on the catalyst surface. Both adsorption energies and activation energies are commonly calculated using electronic structure calculations. The computational costs for calculating adsorption and surface reaction energetics are high, largely due to the high costs of calculating the electronic structure of the solid. For reaction energetics (including adsorption energetics), descriptor-based approaches can be employed to mitigate computational costs: in these approaches, more easily obtained values are used to estimate the quantity of interest based on an empirical or scientifically informed correlation. The quantity used is often a change in electronic energy for a reaction, ΔE_{rxn}, which is the same as the 0 K ΔH_{rxn}°. For most reactions (including adsorption and desorption), ΔE_{rxn} is the main component of ΔH_{rxn}° even at elevated temperatures under reaction conditions, such that typically $\Delta E_{ads,H} \sim \Delta H_{ads,H}^{\circ}$. Thus, from a conceptual point of view, an experimentalist can consider ΔE_{rxn} to be similar to ΔH_{rxn}°. Various electronic-structure-based chemical descriptors and linear relations have been shown to be successful for reactions over metal oxides,[12,19−23] including oxygen vacancy formation energies (ΔE_{vac}) and hydrogen adsorption energies

Received: April 13, 2023
Revised: June 15, 2023
Published: July 6, 2023

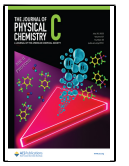

https://doi.org/10.1021/acs.jpcc.3c02470
J. Phys. Chem. C 2023, 127, 13451−13465

($\Delta E_{H,ads}$). ΔE_{vac} refers to the energy of removing a lattice oxygen (which is related to the energy required for refilling oxygen vacancies ($-\Delta E_{vac} = \Delta E_{refill}$), and $\Delta E_{H,ads}$ refers to the energy for creating a hydrogen atom on the surface by adsorption from the gas phase (typically using H_2 gas as a reference state). ΔE_{vac} and $\Delta E_{H,ads}$ have been shown to be "universally correlated" to C−H activation energy in alkanes and oxygenates over a wide variety of metal oxides.[24] Recent DFT calculations using a Brønsted−Evans−Polanyi relationship for H abstraction for methane by a surface oxygen suggest a late transition state (meaning a more radical-like transition state).[24] This finding of a late transition state can be used to rationalize the C−H activation correlation with $\Delta E_{H,ads}$: $\Delta E_{CH_3,ads}$ is nearly linearly related to the height of the barrier by the BEP correlation, and $\Delta E_{CH_3,ads}$ is in turn correlated to $\Delta E_{H,ads}$ for electronic structure reasons.[25,26] Descriptors and other linear relationships for reactions on oxides have also been found for alcohol dehydration,[13,27] ether decomposition,[13] and ether formation.[27]

In general, descriptors currently do not achieve as much accuracy as would be necessary to be true substitutes for electronic structure calculations (this issue is further discussed in the section titled "Alkane CH Bond Breaking Reactions"). Bulk electronic properties of oxides,[11] bulk reducibility enthalpies,[28] band gaps,[29] and geometric descriptors[30,31] have also been shown to be useful descriptors for metal oxide catalyzed reactions and are part of the progress toward multiterm equations that can accurately predict energetics of surface reactions on oxides, which will likely involve compressed sensing methods.[32,33] There is presently an opportunity to enrich such efforts through more experimental measurements of surface energetics such as those of surface oxygen vacancy creation. The lack of experimental databases of accurate measurements represents a significant gap to be filled for progress.[34,35] Various experiments could help to fill this gap, even with some being less accurate. For example, oxide nanocrystals[36] could be utilized in gas−solid powder calorimetry experiments[37−43] or liquid−solid calorimetry experiments.[44,45] Additionally, databases could also include energies indirectly estimated from temperature-programmed reaction[46−49] experiments. Adsorption enthalpies, oxygen vacancy formation energies, and activation energies can depend on surface coverage/concentration. Accordingly, databases should be created with the intent of accommodating coverage dependent values.

METAL OXIDES AS LEWIS ACIDS/BASES AND ATOM ABSTRACTORS

Atom abstraction typically occurs in a separate elementary reaction step after adsorption of a gas phase reactant on the surface. In the adsorption step, oxide surfaces can act as Lewis acids/bases, which can modulate the electronic energetics to enable atom abstraction. Metal oxides can act as *Lewis acids*—as an example, when a carbonyl molecule adsorbs on the cation of a metal oxide, there is electron donation to the cation, and this interaction is important in the activation of carbonyl compounds on metal oxides. Metal oxides can also act as a *Lewis base*—as an example, when an alcohol adsorbs molecularly, the hydrogen atom from the hydroxyl group often coordinates with a surface anion.

A common practice in the literature is to discuss adsorbates on polar surfaces as if they are anions and cations. The common practice of referring to hydrogen atoms on oxygen anions as "protons" or "radical-like" can cause misconceptions.[50] We are not aware of any cases where there is a significant extent of radical character reported for hydrogen adsorbed on a metal oxide surface (that is, with an unpaired spin localized on the hydrogen). It is useful to imagine adsorbed hydrogen as being in a state that exists on a spectrum: this spectrum ranges from "proton-like" (has a partial positive charge, designated as H^+) to "atom-like" (approximately neutral but still sharing electrons, designated as H^0) to "hydride-like" (has a partial negative charge, designated as H^-). Present day electronic structure codes can extract the extent of radical character of a surface bound hydrogen atom using site projected spins (which can be non-integer). The adsorbed species non-integer charges commonly have absolute magnitudes ranging from +0.05 to +1.00.[30,51] It will be interesting if further systematic studies can be conducted to investigate correlations with charges of surface adsorbates (as well as surface lattice atoms) for specific reactions across catalyst series.

For some oxides, termed reducible oxides, a fraction of the lattice oxygen atoms may be removed through redox reaction steps to create oxygen vacancies, which can then be refilled by oxygen atoms in subsequent reaction steps to complete a catalytic cycle. Such mechanistic steps enable the surface to supply and/or abstract oxygen atoms during a reaction, as in some of the reactions described further below. Mechanisms including such steps are said to be Mars van Krevelen mechanisms and are well studied. However, there is still a need to comprehensively study why some oxygen vacancies are effective for deoxygenation reactions, while other oxygen vacancies are not effective for deoxygenation reactions. Presumably, both electronegativity and geometric factors will need to be considered for a comprehensive understanding.

ALKANE C−H BOND BREAKING REACTIONS

C−H activation in alkanes has societal importance, and it is often desired to activate only one C−H bond per alkane molecule (to create alcohols or coupling to larger alkanes). However, it is chemically challenging to activate one C−H bond per alkane molecule without activating further C−H bonds per alkane molecule. The elementary step for C−H activation follows one of two general mechanisms on metal oxides (Figure 1). In the first possibility, there is C−H abstraction by surface

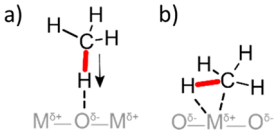

Figure 1. There are two mechanisms for C−H bond breaking on metal oxides: (a) direct H abstraction; (b) metal atom insertion. The metal atom insertion route brings the molecular center of the methane molecule closer to the surface than the geometry of simple adsorption. For both panels, the bond shown in red is the C−H bond that is being broken.

oxygen to form two surface intermediates, an adsorbed hydrogen species and an adsorbed CH_3 species, where the $CH_3^\bullet$ desorbs subsequently and reacts in the gas phase. The second possibility occurs when a metal cation inserts into a C−H bond and forms a C−M bond, while the hydrogen is (typically) transferred to a nearby oxygen. In either case, the final adsorbed hydrogen ends up with a charge closer to H^0 (with electron density located at the hydrogen) or more like a H^+ (with electron density depleted from the hydrogen). In addition

https://doi.org/10.1021/acs.jpcc.3c02470
J. Phys. Chem. C 2023, 127, 13451−13465

to the two general mechanisms, concerted or neighbor-influenced variations are also possible (as has been seen for the four-center transition state in methane C−H bond breaking over PdO in Figure 13 of ref 52).

For the direct abstraction type of methane activation (Figure 1a), several studies have found CH activation to occur via a late transition state (such that the transition state is typically more like the dissociated state with CH_3 and H species), and this is reflected in BEP relationships.[15,17,24] Reaction 4 can be thought of as heterolytic C−H activation, though a highly uncoordinated surface M atom could bind to both the C and H at the transition state such that the activation process is more homolytic in nature.

To activate C−H bonds via direct H abstraction at low temperatures (<500 °C), a strongly oxidizing surface site is required to abstract and adsorb the H atom. This type of site can be made by "forcing" a surface metal atom into an unstable higher oxidation state, such that the adjacent surface oxygens are unstable. One strategy for achieving this is by substitutional doping, which pushes the state of the oxygens neighboring the doped cation to a different position along the descriptor line (see Figure 2 for doping of CeO_2).[53] For example, Pd−ceria systems have exhibited the best performance at low temperature (<400 °C) methane catalytic combustion,[54] and this system involves relatively unstable Pd^{4+} cations.[55] The same type of trend as Figure 2 was seen for cation doping of Co_3O_4.[21]

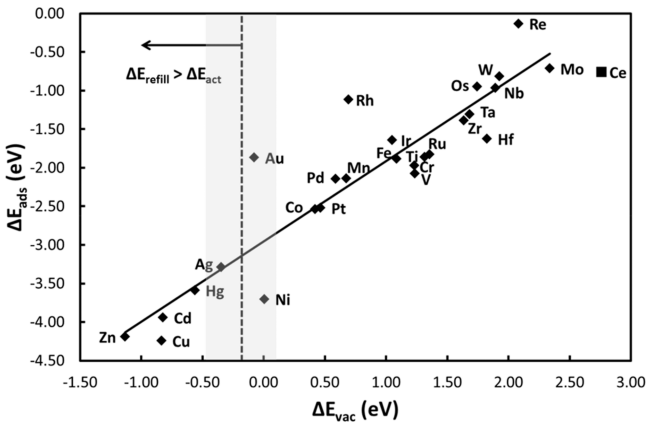

Figure 2. On CeO_2 and substitutionally doped CeO_2, the direct H abstraction route with dissociative adsorption of methane is operative. For this system, the electronic energy of reaction for dissociative adsorption of methane (ΔE_{ads}) serves as a measure of the ease of methane activation, with a more negative ΔE_{ads} indicating easier methane activation. Plotting this descriptor (ΔE_{ads}) versus the oxygen vacancy formation energy (ΔE_{vac}) is instructive to see how substitutional doping to change ΔE_{vac} affects methane activation for transition-metal-doped $CeO_2(111)$ surfaces. Each data point indicates the position for after doping that transition metal into the ceria, with the cation doped into a cerium lattice position in the surface of a 2 × 2 cell. ΔE_{ads} is the electronic portion of $\Delta H_{rxn}°$ for dissociative methane adsorption, such that $\Delta E_{ads} \sim \Delta H_{ads,dissociative}°$. ΔE_{vac} is the electronic portion of $\Delta H°$ for oxygen vacancy formation and is the major component of ΔH_{vac}, such that $\Delta E_{vac} \sim \Delta H_{vac}°$. The point for pure $CeO_2(111)$ is labeled as a square. The energy to refill oxygen vacancies ($-\Delta E_{vac} = \Delta E_{refill}$) from $O_2(g)$ at 0 K is greater than the methane activation barrier to the left of the dashed line. Thus, to the left of the dashed line, reoxidation would be the rate-determining step within a methane oxidation catalytic cycle at any O_2 pressure. Reprinted and adapted with permission from ref 53. Copyright 2012 Elsevier.

A more reducible oxide, with a less endothermic oxygen vacancy formation energy, is more active for dissociating C−H bonds. However, for mechanisms which involve removing surface oxygens during an oxidation reaction, making a catalyst that is even more active, or active at lower temperature, is challenging in that a more reducible surface would be unfavorable to reoxidize. Within Figure 2, there will be an optimal position along the descriptor line that balances C−H bond activation with catalyst reoxidation for any given set of conditions. The relative O_2 and CH_4 pressures will impact the position of the "volcano peak"; however, as chemical potential is only logarithmically dependent on pressure, even a 100 bar pressure difference alters the optimal material by only ∼0.3 eV at 800 K (and even less at lower temperatures). The shaded region of Figure 2 shows then the optimal range, and a practical catalyst might feasibly be found within or near this region.

There is a need for greater accuracy when developing such relations. DFT methods overestimate the O−O bond formation energy in molecular oxygen by more than 0.5 eV,[6] and values in Figure 2 are not corrected for this error. DFT at the generalized gradient approximation level suffers from unignorable electron self-interaction errors, especially for lanthanides and actinides. The data in Figure 2 include Hubbard U corrections on Ce f states, but U values are empirical corrections where a single U value will generally predict one property more correctly at the expense of another property (such as adsorption energy versus bandgap), and a single U value may not be accurate for two different structures. The O vacancy formation energy for the $CeO_2(111)$ surface varies by ∼1.5 eV as the U correction for Ce f states is varied from 3 to 7.[56] Varying the U value on Mn d-states from 0 to 5 changes the O vacancy formation energy for the Mn-doped $CeO_2(111)$ surface by ∼1 eV and alters whether Mn takes on a formal +2 or +3 state in the reduced surface.[57] These DFT inaccuracies introduce significant and difficult to quantify errors, and methods are needed to overcome these challenges. Bayesian parameter estimation in chemical kinetic modeling and design of experiments may help to improve upon the uncertainties for DFT calculated quantities,[58−60] but it requires comparison to experiments. A promising way to achieve more accurate electronic structure calculations that is currently under active research and will likely make a big impact is machine-learning corrections to energetics from electronic structure calculations, though it will only be possible once accurate training sets are available. Such corrections can include nuances of chemical environments such as the positions of nearby atoms and other factors.

The metal atom insertion mechanism (Figure 1b) presents additional opportunities. This mechanism (like the direct H abstraction mechanism) generally involves cations in less stable "overoxidized" states to activate a C−H bond. The metal cation (or single atom) must be sufficiently exposed (for steric access) and coordinatively unsaturated (for electronic bonding). Palladium oxide catalysts have been proposed to activate C−H bonds through the insertion mechanism by undercoordinated Pd atoms on PdO(101) facets.[61,62] In the metal insertion mechanism, as with the H-abstraction mechanism, facilitating selectivity to any products other than CO and CO_2 at lower temperature remains a challenge.

For both types of mechanisms, when the activity is described by a linear scaling relationship, there is an upper bound to the activity possible due to "volcano" behavior with activity versus the descriptor.[63] Accordingly, there is desire to go "beyond" known linear scaling relations, and this process is referred to as

https://doi.org/10.1021/acs.jpcc.3c02470
J. Phys. Chem. C 2023, 127, 13451−13465

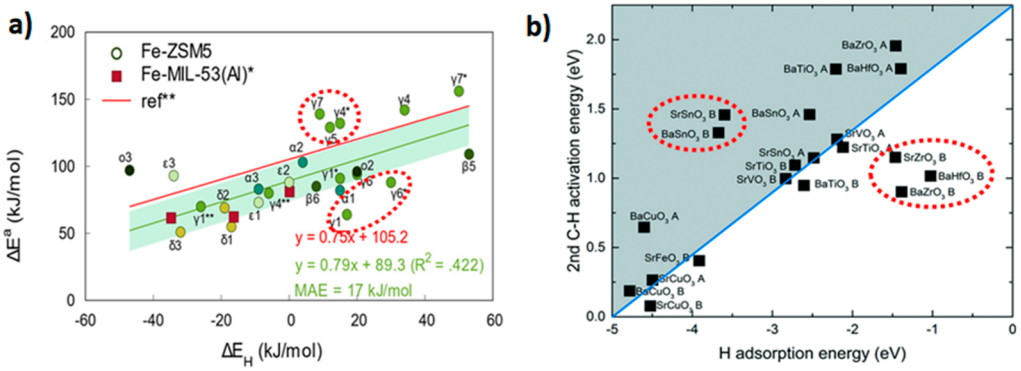

Figure 3. Graphical demonstration of successful strategies to break scaling relationships for C−H activation. The energies represent electronic energies. Red dashed ovals indicate regions where catalysts have been found that deviate from the scaling relations. (a) Breaking the scaling relation for the first C−H activation (via confinement effects). (b) Breaking the scaling relation for the second C−H activation (via modulated surface composition). In the left panel, ΔE_H is the electronic $\Delta H_{rxn}°$ for hydrogen atom adsorption, and $\Delta E_H \sim \Delta H_{ads,H}°$. Left panel adapted with permission from ref 65. Copyright 2019 American Chemical Society. Right panel adapted with permission from ref 66. Copyright 2018 Royal Society of Chemistry.

"breaking" the linear scaling relations. When alkane oxidation occurs via direct H abstraction, the scaling relationship between C−H activation with ΔE_{vac} and ΔE_H leads to a volcano trend where the activity is correlated with the redox ability of the catalyst.[15,17,24]

Several strategies have been proposed recently which provide plausible approaches to break C−H activation scaling relationships. The most obvious approach to breaking scaling is to use catalysts that shift the mechanism to an alternative scaling line (such as from direct C−H abstraction to metal insertion).[15,22,64] Another method is by controlling the active site environment to favor or disfavor a particular transition state or intermediate via confinement or cooperative interactions. The scaling between methane C−H activation and ΔE_H was broken by dual effects in a Fe-ZSM-5 catalyst (Figure 3a).[65] The confinement of the zeolite pore reduces the geometric flexibility of the methane and destabilizes the transition state, while cooperative interactions from nearby OH groups have an opposite effect and stabilize the transition state. These opposing levers result in trends more complex than a single linear relation.

Breaking scaling relations is also important for selective production of partial oxidation products (such as methanol from methane), as it requires the catalyst to be selective to the first C−H bond and not to undergo further C−H bond breaking. This goal is challenging as the C−H bond dissociation energy of methane is higher than that of methanol. Similar challenges plague other alkane conversion processes such as propane dehydrogenation and methane oxidative coupling. A potential viable strategy around this problem is that the second C−H activation of methane can be inhibited on the surface in certain cases due to steric or electrostatic influences (Figure 3b).[66] This could prevent surface bound intermediates from undergoing runaway oxidation prior to desorbing and forming products such as ethane from coupling in the gas phase. Single atom catalysts have been found to prevent further C−H activation of alkanes in a similar manner by providing only a single isolated site for facile C−H activation.[67] Deactivating or poisoning sites relating to overoxidation have also yielded promising results, such as using water to prevent formation of active oxygen species in a CeO_2−Cu_2O catalyst.[68] While the above cases can prevent overoxidation of adsorbed intermediates, they typically do not solve the problem of further oxidation, which occurs via gas phase product readsorption. The current strategies that seem viable for preventing overoxidation from readsorption are enzymatic-like sites or reactor engineering. From the reactor engineering perspective, overoxidation can be mitigated by use of gas-phase "collectors", aqueous reaction environments, or diffusion limited systems—which could potentially keep the primary product away from the reaction site.

C−H BOND BREAKING IN ALCOHOLS AND ALDEHYDES

H abstraction from organic oxygenates is well studied for metal oxide catalysis.[5,7] For an empty surface, organic oxygenates typically adsorb with oxygen interacting with a surface cation, and for alcohols and organic acids, the O−H bond typically dissociates upon adsorption. There are typically two types of C−H bonds: (1) those on non-oxygenated carbons that are only bonded to other carbons and hydrogens (RCH_3), which are chemically similar to aliphatic C−H bonds, and (2) those that are on oxygenated carbons and include bonds to oxygens within the molecule (RCH_xO_y).

From a molecular orbital point of view, the C−H bond breaking on the non-oxygenated carbons (of alcohols, aldehydes, and organic acids) is chemically similar to C−H bond breaking on alkanes.[69] Indeed, a single relationship has been found to describe both alkane dehydrogenation and alcohol dehydration over γ-Al_2O_3, as the alcohol dehydration requires breaking a beta carbon C−H bond, which behaves sufficiently similar to breaking an alkane C−H bond.[49] There are two principle routes for losing the beta hydrogen from an alcohol: (a) the route where two H atoms and one O atom are lost from the molecule (that is referred to as "dehydration") to create an alkene and (b) the route where two H atoms are lost from the molecule (that is referred to as "dehydrogenation") to make an aldehyde. Alcohol dehydration and dehydrogenation have been studied over many oxides,[13,70,71] and trends associated with the electronegativity of surface atoms and other descriptors have been published.[11,71−81] Over reducible oxides, the route to "dehydrogenate" an alcohol to an aldehyde can in fact make H_2O as a coproduct (rather than molecular H_2) if a surface lattice O is removed during reaction, and such an observance of H_2O should not be confused with the above usage of the word "dehydration", which refers to the removal of an oxygen from a reactant molecule. The situation is further complicated because an aldehyde can be deoxygenated by some

https://doi.org/10.1021/acs.jpcc.3c02470
J. Phys. Chem. C 2023, 127, 13451−13465

catalysts, in which case there is a dehydrogenation followed by a deoxygenation, which is stoichiometrically equivalent to a dehydration and can be called a net dehydration reaction.

For C−H bond breaking on the oxygenated carbon (such as the CH_2 in CH_3CH_2OH), both direct C−H bond breaking (H abstraction by a surface lattice oxygen) as well as disproportionation (H abstraction by a neighboring adsorbate molecule's oxygen) were hypothesized to be plausible over metal oxide surfaces, each believed to occur via alkoxy intermediates. Experimental evidence supported the possibility of both routes, but it has been generally assumed that both routes involved modest activation barriers that could not be accessible until >300 K. However, experiments over $CeO_2(111)$ have recently been analyzed with electronic structure calculations and kinetic Monte Carlo simulations to show that the <300 K formaldehyde production was consistent with a below room temperature C−H bond breaking with an elementary step involving a disproportionation reaction (Figure 4), with the two intermediates adsorbed

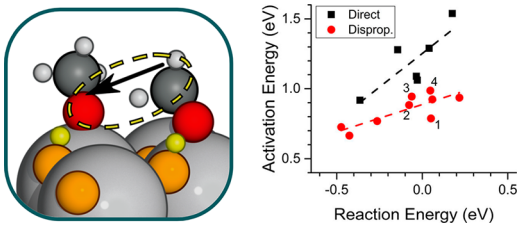

Figure 4. Left panel: A disproportionation reaction between neighboring on-top methoxy adsorbates on $CeO_2(111)$, where there is a hydrogen being abstracted from the methoxy on the right. The methoxy on the left will become a methanol molecule after receiving the hydrogen, while the methoxy on the right will become a formaldehyde molecule. Atom colors: C - dark gray, adsorbate H - white, adsorbate O - red, lattice Ce - light gray, surface lattice O - orange, surface adsorbed H - yellow. Right Panel: Both the direct H abstraction route and this new H abstraction by disproportionation follow BEP relationships, which longer chain alcohols also follow. Adapted with permission from ref 20. Copyright 2017 American Chemical Society.

on non-vacancy surface sites.[20] While this low temperature disproportionation route was found over cerium oxide, it seems likely that this transition state exists over other oxides as well.

Another case where C−H bond breaking involving a neighboring adsorbate has been found is a pseudo-disproportionation mechanism for conversion of ethanol to acetaldehyde over $La_{0.7}Sr_{0.3}MnO_{3-x}(100)$.[82] In this example, an oxygen atom from the surface serves to shuttle the hydrogen between the neighboring adsorbates (Figure 5). The two above examples demonstrate that neighboring adsorbates can be important in C−H bond breaking during conversion of alcohols.

CC COUPLING IN ALCOHOLS, ALDEHYDES, KETONES, AND ORGANIC ACIDS

Today, C−C coupling is of particular interest when catalytically converting organic oxygenates over metal oxides. Converting biomass derived organic oxygenates into high energy density fuels that are compatible with existing transportation infrastructure involves removal of oxygen and also C−C coupling.[83,84] Alcohols almost never directly couple. Instead, alcohols are generally oxidized to aldehydes or organic acids which then undergo C−C coupling reactions.[85,86] Accordingly, in this section, we will focus on the carbonyl compounds,

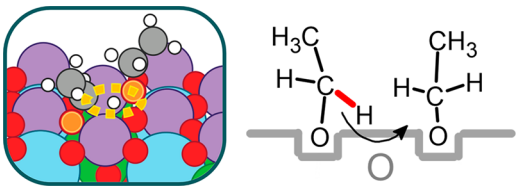

Figure 5. Pseudo-disproportionation reaction between alkoxies on neighboring vacancies over $La_{0.7}Sr_{0.3}MnO_{3-x}(100)$, assisted by a lattice oxygen. The left panel shows the transition state for this new pathway, with H abstraction from the alkoxy on the left and the hydrogen being transferred to the alkoxy on the right. Left panel atom colors: H - white, C - gray, Mn - purple, Sr - green, La - blue, oxide lattice O - red, molecular adsorbate O - orange. Left panel adapted with permission from ref 82. Copyright 2020 American Chemical Society.

recognizing that alcohols can be relatively easily oxidized to aldehydes and to carboxylic acids.

Aldehydes and Ketones. With carbonyl compounds, the most typical mechanism for catalyzed C−C coupling over oxides is aldol condensation. Two carbonyls (or their enol tautomers) interact, with one acting as a Lewis acid and the other molecule acting as a nucleophile (see attached reference for more details on the coupling step).[87] Historically, the aldol addition paths were described as either "acid catalyzed" or "base catalyzed". However, on oxide surfaces, the adsorption and reaction typically occur with bifunctional site ensemble interactions. Thus, aldol additions on surfaces typically involve both acid and base sites, and a more general terminology is the nucleophile^electrophile nomenclature.[87] In this nomenclature, the types of the two coupling intermediates are specified: the type of intermediate acting as the nucleophile appears first, and the type of intermediate acting as the electrophile appears second, with a "^" in between. For example, Enol^Kketo refers to a C−C coupling where the nucleophile is an enol species and the electrophile is a keto species.

When carbonyl compounds adsorb on metal oxides the oxygen of the carbonyl interacts with a Lewis acid or Brønsted acid site, and the withdrawal of electrons by the acid site (for either type of acid site) moves the carbon within the C═O to a greater carbocation character. This electronic change makes the carbon more susceptible to nucleophilic attack. For most cases of aldol addition over oxides, evidence based on isotopic labeling and kinetic studies suggested that aldol addition occurred via an enolate created by extraction of a hydrogen from the aldehyde, followed by the Enolate^Keto mechanism.[87,88] A DFT calculated transition state for this elementary step is shown in the upper half of Figure 6 for $CeO_2(111)$. Typically, it is assumed that the rate-limiting step is at or before C−C coupling, and catalysts tend to be deactivated by carbonaceous deposits created by further polymerization reactions.

However, it was speculated that it would be possible to have aldol coupling with enolates bound in oxygen vacancies. Using a series of designed temperature ramps and gas exposures, researchers succeeded in creating a situation with both aldehydes and enolates in vacancies on partially reduced $CeO_2(111)$ and achieved crotonaldehyde production from these species.[87] The reaction occurs from intermediates on adjacent surface oxygen vacancies with an X^+−Enolate^Keto mechanism (Figure 6), based on DFT calculations and kinetic simulations.[87] An open question is whether this oxygen-vacancy-based X^+−Enolate^Keto mechanism has the potential to enable more selective coupling and avoid deactivation. If it can,

https://doi.org/10.1021/acs.jpcc.3c02470
J. Phys. Chem. C 2023, 127, 13451−13465

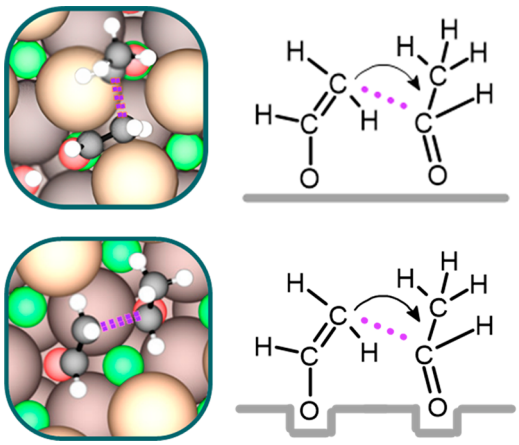

Figure 6. Aldol addition of aldehydes over $CeO_2(111)$. Upper panel: transition state of aldol addition through an Enolate^Keto mechanism over a nonreduced surface of $CeO_2(111)$, where the aldehyde and enolate are each adsorbed at surface lattice Ce sites. The dashed purple designates bond formation. Lower panel: transition state of aldol addition through an X^+−Enolate^Keto mechanism over a reduced surface of $CeO_2(111)$, where an aldehyde and enolate each adsorbed at surface oxygen vacancy sites. The dashed purple designates bond formation. Atom colors: C - black, H - white, adsorbate O - red, lattice Ce - green, surface lattice O - light brown, subsurface lattice O - dark brown. Upper left panel adapted with permission from ref 89. Copyright 2021 American Chemical Society. Lower left panel adapted with permission from ref 87. Copyright 2019 American Chemical Society.

computational calculations and simulations are sufficiently advanced that it should be possible to "screen" plausible systems and conditions that may enable this mechanism to be dominant during steady state reactions over catalysts.

Carboxylic Acids. Organic acids have more than one possible mode of adsorption on oxides, and organic acid coupling has more than one possible mechanism even within particular modes of adsorption. The dominant mechanism can shift with the presence of coadsorbates, surface coverage, and the number of vacancies on the surface. These complications make mechanistic studies challenging. Catalyzed reactions of organic acids have been reviewed,[90−92] though unresolved mechanistic complications remain.

Ketones can be produced from carboxylic acids via three pathways that are highly dependent on the catalyst type. Alpha hydrogen abstraction is essential for ketonization chemistry,[93,94] with CO_2 release occurring later (during or after the coupling step). Evidence has suggested that the rate-limiting step is typically C−C coupling. Two classes of transition states for the C−C coupling step are often proposed, both of which involve an acetate enol (or its conjugate acid). The two classes of transition are shown in Figure 7, where the left panel depicts an acetate coupling with an acetate enol and the right panel shows an acyl cation coupling with an acetate enol.[95−99] The case in the left panel may involve H_2O production after coupling, while the case in the right panel involves H_2O production before coupling.

Various adsorbate configurations are possible when considering that there can be molecular acetic acid versus dissociatively adsorbed acetic acid and also various combinations of surface oxygens, surface hydroxyls, oxygen vacancies, and cation coordination (Figure 8). An acetate group can be monodentate-coordinated, bidentate-coordinated, on a more or less coordinated cation, or even on a surface hydroxyl and may have

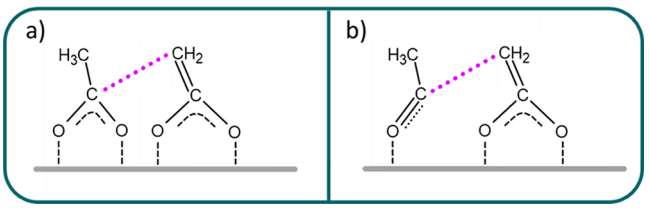

Figure 7. Two distinct classes for C−C coupling transition states during the coupling reactions of carboxylic acid derived species: (a) an acetate type electrophile coupling with an acetate−enolate nucleophile; (b) an acyl type electrophile coupling with an acetate−enolate nucleophile. Some of the other type of local adsorbate configurations are shown in Figure 8 for acetate and acetate−enolate intermediates.

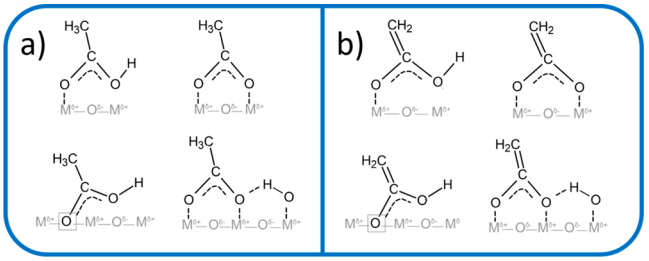

Figure 8. (a) Example local configurations for acetates (typically the electrophile). (b) Example local configurations for an acetate−enolate (typically the nucleophile). When considering the possibilities of molecular adsorption, dissociative adsorption, oxygen vacancies, neighboring hydroxyls, and different surface sites, there are tens of possibilities for the bimolecular coupling elementary step. The set of possibilities shown is not comprehensive. For example, the case of two oxygen vacancies is not shown, and the case of being bound to only a hydroxyl is not shown. The full number of possibilities will also include acyl species, methylene species, and aldehydes.

the acetate's oxygens residing in oxygen vacancies. Experiments and calculations suggest that oxygen vacancies may play a significant role on this chemistry.[96,100] The situation is further complicated by the possibility of hydrogen bonding with neighboring adsorbates or surface hydroxyls. The binding mode will vary both with acid coverage as well as reaction environment.[100] It is very challenging to discern from experiments which class of transition state is involved and even more challenging to discern what exact configuration is involved. These scenarios present tens of possibilities, which also presents a difficult challenge for electronic structure calculations.

A recent DFT study[99] showed compelling evidence for a transition state of the class of transition states on the left side of Figure 7 for acetic acid coupling over anatase $TiO_2(110)$. The calculations also showed that higher acid coverages stabilized the initial adsorbate state while also lowering the barrier for coupling. The authors conclude that the H-bonding interactions are important. This mechanism was consistent with kinetic isotope studies and DFT calculations over unreduced TiO_2 and ZrO_2 catalysts.[100] Thus, far, no study has provided a comprehensive elementary step explanation that reproduces both the effects of coverage dependence and the effects of varying degrees of surface reduction.

The age-old geometric vs electronic arguments tend to persist with this chemistry, and our abilities to identify the true underlying nature of the proposed chemistry are rapidly advancing with improved characterization and theory. As machine learning augmented electronic structure calculations increase in accuracy[101] and advances are made in ab initio

https://doi.org/10.1021/acs.jpcc.3c02470
J. Phys. Chem. C 2023, 127, 13451−13465

molecular dynamics,[102] these simulation methods as well as kinetic Monte Carlo[103] methods will enable a more full understanding of what occurs on any given surface under a given set of conditions. Conclusions about the dominant reactive adsorbate species must be carefully interpreted to be condition dependent. To better understand these effects, experimental evidence contrasting the role of coadsorbed species, in particular surface OH groups and water, should be explored further at varying acid coverage.

OXYGENATE REACTIONS OVER CONFINED ACID SITES

Dehydration of Alcohols over Confined Acid Sites. Alcohols can be dehydrated to form alkenes over Brønsted sites. This reaction has been relatively well studied by electronic structure calculations and experiments, such that the mechanism is well understood at the elementary step level (Figure 9).[104,105]

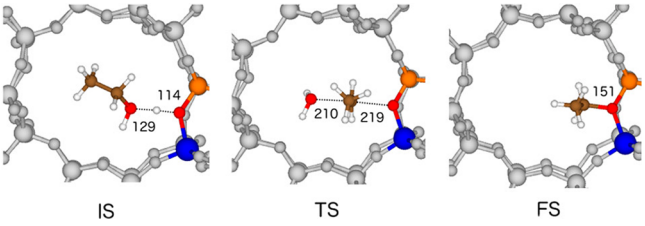

Figure 9. Initial state (IS), transition state (TS), and final state (FS) for dehydration of ethanol by H-ZSM-5. The newly formed water molecule is not shown in the final state panel. Bond lengths are given in pm. Atom colors: C - brown, H - white, O - red, Si - orange, Al - blue. Figure adapted with permission from ref 104. Copyright 2018 American Chemical Society.

A complex is formed in which the acidic Brønsted hydrogen is either coordinated with the alcohol or the Brønsted hydrogen is transferred completely to the alcohol, with the newly formed species (referred to as a "protonated alcohol" in the literature) remaining coordinated to the newly formed basic site.[106] The energy difference between these two cases of interaction (Brønsted hydrogen transferred versus not transferred) is small (<10 kJ/mol),[106] and experimental researchers typically do not know which of the two cases are occurring: indeed, the two states may be in equilibrium. Accordingly, we will use the term "Brønsted-coordinated" to encompass both types of states, rather than distinguishing between the two states. Density functional theory (DFT) calculations on Brønsted-coordinated butanol in H-MFI showed that van der Waals interactions with the zeolite were the dominant source of adsorption enthalpy, which explains the relatively small energy difference between these two extremes.[106]

The interaction enthalpy includes contributions from multiple terms: hydrogen bonding, Coulombic interaction(s), and dispersive (van der Waals) interactions. A quantitative understanding of some of these factors can be gained by considering a Born−Haber thermochemical cycle including alcohol adsorption and the abstraction of hydrogen from the acid site. This method enables separation of the local environmental contribution ($\Delta H_{interaction}$) from the total enthalpy of adsorption (ΔH_{ads}). Using a Born−Haber thermochemical cycle with values derived from DFT calculations of the adsorption of butanol isomers on H-ZSM-5, it was shown that both steric interactions and van der Waals interactions influenced the enthalpy of adsorption.[106]

A similar approach was used to study the adsorption of a broader range of alcohols on zeolites using DFT, with inclusion of van der Waals corrections.[104,107] For H-ZSM-5, the initial and final states as well as the transition state for the dehydration of small alcohols are surprisingly well described by a linear correlation between the total DFT energy and van der Waals energy as shown in Figure 10a.[104] Further, because it is possible

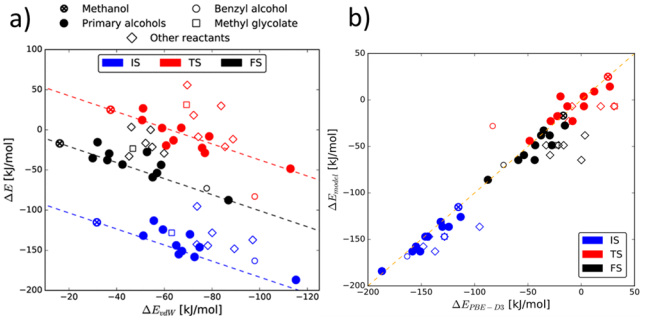

Figure 10. (a) Correlation between total energies calculated by PBE-D3 density functional theory (vertical axis) vs the D3 van der Waals contribution (horizontal axis) for relevant states. (b) Parity plot when predicting relevant state energies using an empirical algebraic model to approximate the van der Waals contribution and the explicitly calculated PBE-D3 energies. The following three series of energies are plotted: (i) energies of the initial states (blue), (ii) final states (black), and (iii) transition states (red). Filled circles represent cases with primary alcohols as reactants, while open symbols represent cases with other alcohols that include the steric and electronic effects from additional functional groups. Images adapted from ref 104. Copyright 2018 American Chemical Society.

to empirically predict the van der Waals energy by algebraic empirical correlations, the various state energies, including the transition state energies, can also be well predicted by an algebraic model, as shown in Figure 10b. These correlations mean that some portions of chemical kinetic modeling can be performed without explicit electronic structure calculations. Thus far, this powerful approach has not been generalized, but it would have significant ramifications if successfully generalized.

C−C Bond Formation with Aldehyde Reactants/Intermediates over Confined Acid Sites. For aldehydes, there are two major classes of Brønsted acid site catalyzed C−C coupling reactions that can be utilized to build larger molecules: (i) aldehyde−aldehyde coupling in aldol condensation and (ii) aldehyde−alkene coupling in Prins condensation. Both reactions can occur in zeolites by an aldehyde adsorbed on a Brønsted acid site and can be modulated by confinement effects. Confined environments are particularly important for coupling reactions, since the size of the C−C bond formation transition state is approximately twice of that of the reactant state.

DFT calculations show evidence of partial proton transfer (or "sharing") of the proton from the zeolitic Brønsted hydrogen and adsorbed aldehyde acceptor.[108] The ability for the aldehyde to "take" (or partially take) the Brønsted hydrogen facilitates the coupling reactions by creating an aldehyde with stronger carbocation character. The proton affinity of aldehydes (defined as the negative of the enthalpy change of the aldehyde reaction with a free proton in the gas phase) gives insight into their total heat of adsorption on Brønsted acid sites (since Brønsted acid sites are chemically similar to protons). Aliphatic aldehydes ($C_nH_{2n}O$) exhibit similar gas phase proton affinities to those of aliphatic alcohols ($C_nH_{2n+1}OH$) as a function of carbon chain

https://doi.org/10.1021/acs.jpcc.3c02470
J. Phys. Chem. C 2023, 127, 13451−13465

length; that is, aldehydes and alcohols have very similar Brønsted base strengths at their oxygen atoms.[109,110] The trend of proton affinities with chain length is also the same for aldehydes and alcohols, with rather small quantitative differences between the two types of molecules. As the alcohols and aldehydes have similar proton affinities, and the alcohols and aldehydes are also of similar size, the same type of pore interactions may occur for Brønsted-coordinated aldehydes, as those which have been shown to occur for Brønsted-coordinated alcohols. These insights suggest that we can expect some similar effects from Brønsted zeolite catalyzed reactions of aldehydes (relative to those of alcohols), despite the different functional groups. We are not aware of any studies making such comparisons, and it is an opportunity to build scaling relations spanning these two functional groups (with a correlation between the enthalpy of adsorption and the enthalpy of H addition to the oxygen as a possible starting point).

When coupling reactions occur for aldehydes with more than two carbons, the effects of pores on pathway selectivity become even more important. For conversions of butanal at atmospheric pressure and moderate temperatures (473−673 K), carbon−carbon bond formation and the elimination of an oxygen heteroatom occur via three parallel catalytic cycles, each of which creates different types of carbon−carbon bonds and leads to different products. The three cycles are (1) intermolecular C═C bond formation between two aldehydes in an aldol-condensation reaction ($C_{2n}H_{4n-2}O$) (Cycle 1), (2) intramolecular C═C bond formation that converts an aldehyde directly to an alkene (C_nH_{2n}) by accepting hydrogen from hydrogen donors (Cycle 2), which can then be followed by Prins condensation between an aldehyde and an alkene,[111] and (3) isomerization−dehydration (Cycle 3a), which involves self-isomerization to an allylic alcohol intermediate before its rapid dehydration to produce an *n*-diene (C_nH_{2n-2}). Cycle 1 includes aldol condensation, whereas Cycles 2 and 3 contain steps that produce alkenes and dienes, respectively, which are reactants for Prins or modified Prins condensation reactions.[112]

The observed rates of the aldol addition step are largely dictated by the rate constant of C−C bond formation and the pre-equilibrium position of the keto−enol tautomerization, and the selectivity has been studied as a function of confinement.[113] On unconfined Brønsted sites, the trend for the alkanal condensation pathway follows the predicted trend from gas phase chemistries, with the effective rate constants for intermolecular C═C bond formation catalyzed by unconfined protons increasing with aldehyde chain length, with the opposite trend shown for inside the pores of H-ZSM-5 zeolites (Figure 11a). The adsorbed, Brønsted-coordinated aldehydes could also undergo a parallel, intramolecular C═C bond formation (Cycle 2) that produces alkenes.[114] Cycle 2 has also been shown to be effected by local confinement around the Brønsted acid sites (Figure 11b).[111,115] The kinetic coupling of the several described catalytic cycles can be modulated by pore effects: several studies have reported the selectivity modulation as a function of pore size.[113,116,117] Specifically, it has been seen that catalysis with confinement (smaller pores) favors Cycles 2 and 3, whereas, without confinement (no pores), Cycle 1 and its secondary reaction Cycle 4 become dominant.

Once alkenes are formed, adsorbed aldehydes on solid Brønsted acid sites can also undergo C−C bond formation with alkenes, via the Prins condensation reaction, forming dienes. The Prins condensation reaction is similar to aldol condensation, in that it involves a nucleophilic attack on the activated

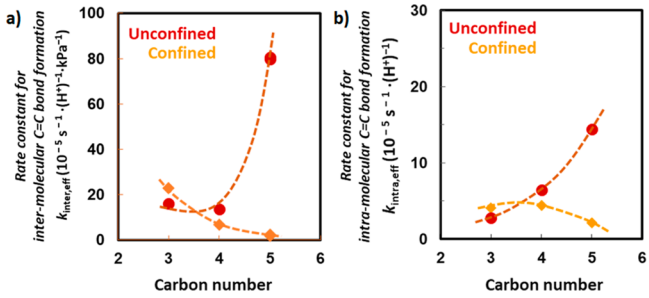

Figure 11. (a) Effective rate constant (first-order) for intermolecular C═C bond formation (Cycle 1) and (b) effective rate constant (zero-order) for intramolecular C═C bond formation (Cycle 2) of aliphatic aldehydes with different carbon number *n* ($C_nH_{2n}O$, *n* = 3−5) on $H_4SiW_{12}O_{40}$ vs H-ZSM-5 catalysts (Si/Al = 11.5) at 473 K (alkanal pressure = 1.1 kPa, TOS = 125 min, space velocity 7.5×10^{-3} s^{-1} on $H_4SiW_{12}O_{40}$, 1.1×10^{-3} s^{-1} on H-ZSM-5).[113,114,117]

carbonyl carbon atom and is catalyzed by Brønsted acid sites, and the initial C−C bond formation is kinetically relevant. The confinement effects can be understood by interpreting the effective rate constant, $k_{prins}K_{al}^{-1}$, within the context of transition state theory, in terms of the activation free energies between the kinetically relevant transition state and the precursor state. The excess activation free energy, defined by the difference in the activation free energies for the reaction, occurred between the confined and unconfined environments, $\mathbf{\Delta\Delta G^{TS\text{-}al}_{confine}}$ ($\mathbf{\Delta\Delta G^{TS\text{-}al}_{confine}} = \mathbf{\Delta G^{TS\text{-}al}_{confine}} - \mathbf{\Delta G^{TS\text{-}al}_{unconfine}}$, where subscripts "confine" and "unconfine" denote the local environment of the acid site at which the reaction occurred), is used as a proxy to quantitatively examine the various effects of confinement. The extent of local confinement was investigated over several microporous and mesoporous structures.[108] As shown in Figure 12, the ensemble-averaged $\mathbf{\Delta\Delta G^{TS\text{-}al}_{confine}}$ value of a catalyst, $\left\langle \overline{\Delta\Delta G^{TS\text{-}al}_{confine}} \right\rangle$, computed by averaging over all distinct O atoms at each Al T-site and then over all T-site locations, mediates its rate constant $k_{prins}K_{al}^{-1}$. While the trend in Figure 12 appears monotonic, it actually arises from the balancing of multiple factors, some of which are competing effects.[108]

The overall catalytic consequence of confinement has multiple "knobs" to tune such as the stabilization by dispersive interactions, host−guest structural distortions, and entropy losses as a result of confinement. The shape of the voids also affects the free energies; for example, in Figure 12, the cage-like intersections in MFI stabilize the activation free energy more effectively than the cylindrical channels of BEA, despite their similar size.

Conversion of Carboxylic Acids over Confined Acid Sites. Carboxylic acids can undergo self C−C coupling ketonization (Figure 13) as well as alcohol C−O coupling (esterification) on strong Brønsted acid sites in zeolites, with confinement also playing a role. On aluminosilicates, more so than other oxide catalysts, the strong Bronsted acids tend to promote dehydration to create surface acyl species (the left species in Figure 7b). These acyl species can couple with adsorbed carboxylic acids to form ketones. Acyl species can also be formed from esters that can serve as intermediates for creation of larger molecules. The role of Brønsted acid sites on organic acid C−C coupling chemistry, including the involvement of acyl intermediates, has been reviewed recently.[91,118]

When aromatic rings are present on intermediates, Friedel−Crafts acylation is another pathway that can occur.[120] Pore

https://doi.org/10.1021/acs.jpcc.3c02470
J. Phys. Chem. C 2023, 127, 13451−13465

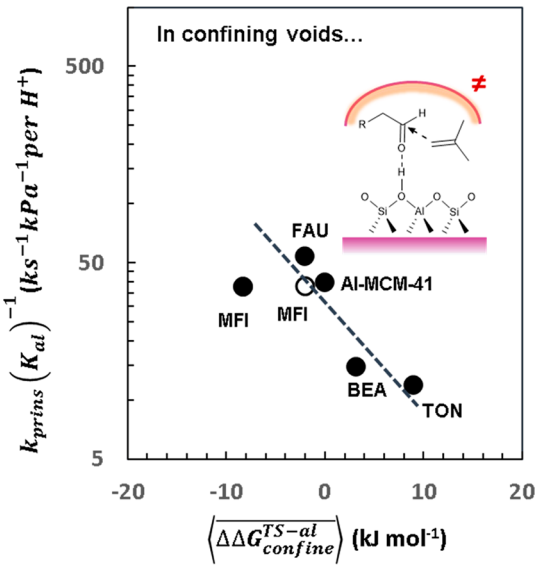

Figure 12. Correlation between the measured Prins condensation rate constant ($k_{Prins}K_{al}^{-1}$, 473 K, 1 bar) versus the change in the Gibbs free energy difference between the kinetically relevant transition state and the precursor state, $\left\langle \overline{\Delta\Delta G^{TS-al}_{confine}} \right\rangle$, of Prins reactions in various aluminosilicate frameworks. Inset: transition state structure of the Prins condensation reaction between a butanal and an isobutene. The energies were derived from ensemble-averaging over all T-site locations (●) of MFI, TON, BEA, FAU, and Al-MCM-41 and all T-site locations of the MFI intersections (○). The dashed line is provided as a visual guide. Adapted from ref 108. Copyright 2017 Elsevier.

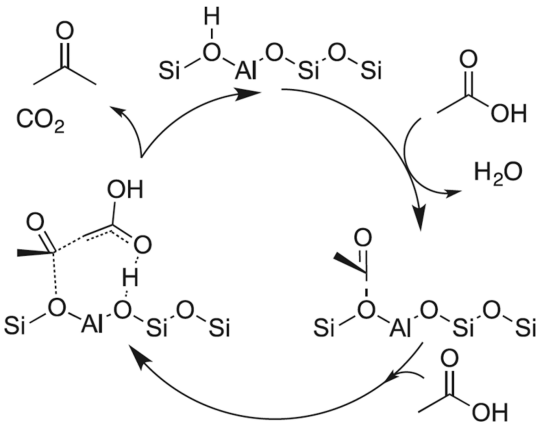

Figure 13. Schematic depicting self-coupling reactions of acetic acid over Brønsted zeolites. Reprinted with permission from ref 119. Copyright 2016 Elsevier.

confinement effects and solvents can stabilize Friedel−Crafts transition states, and influence the rate and selectivity toward C−C coupling reactions.[121] With bulky transition states, small porezeolites can improve intrinsic acylation rates while simultaneously impeding diffusion of intermediates.[122] The use of Brønsted acid zeolites to catalyze dehydration of carboxylic acids is an important direction of advancement over the common and less sustainable use of acyl halides t to facilitate this chemistry. Different proposals regarding the rate-determining step have been presented.[119,121,123]

A recent study revealed that the nature of the acyl acceptor can significantly modify the charge distribution at the transition state and modify rates of C−C coupling.[121] Acyl acceptor molecules, such as cresol or methylfuran, thus facilitate low C−C coupling barriers. This generally shifts the rate-determining step away from C−C coupling to other steps such as the initial dehydration to form the surface acyl species[122] (or anhydride[121]), or to the decomposition of lattice-hydrogen-coordinated products.[124]

A challenge exists in separating rates of diffusion from intrinsic activity, particularly if they have similar magnitudes for rates.[125] For example, MFI zeolites exhibit higher acylation rates than beta zeolites for gas phase reactants, but this was only revealed upon diminishing site density to a very low level such that diffusion does not influence rates. Rates of diffusion of the bulky ester are higher in beta than MFI zeolites, while intrinsic rates of C−C bond formation are higher within the more confined voids of MFI zeolites.[122]

While we have learned much over the past several years about the nature of kinetically relevant transition states associated with acid dehydration and subsequent coupling, the role of confining environment surrounding these transition states as well as the role of acid site proximity are still under investigation. Presently,[104] there are conflicting conclusions about the trends when the rate is normalized to the number of lattice hydrogens in various zeolites. It is not entirely known how the confining environment surrounding active sites plays an important role in stabilizing relevant transition states. Density functional theory calculations and careful experimental studies are needed to understand these phenomena.

SUMMARY AND OUTLOOK

In writing this Perspective, several general themes emerged:

(1) Selective catalytic conversions of organic molecules can benefit from ensembles of sites (consisting of two or more sites). Metal oxides present one route for creating ensembles of sites. For organic oxygenates, such site ensembles have been found to enable accessing transition states that were not otherwise accessed at relevant temperatures.

(2) Within a particular type of site ensemble, subtle chemical changes can have large changes in selectivity and activity. Oxides enable new transition states to be accessed and improved upon from a combination of geometric factors (distances between neighboring molecules) and electronic factors (substitution of anions and cations). The phase space is further broadened by the inclusion of the possibility of oxygen vacancies. It is not always only the solid that is important in abstraction reactions but also the neighboring molecules and intermediates.

(3) Confined environments can be important due to dispersive interactions (which are enthalpic contributions) and also steric constraints (entropic and in some cases also enthalpic) becoming dominant factors in reaction pathway selectivity. These effects are now being increasingly understood, becoming increasingly routine for computational studies, and correlations are being accumulated that hold within specific series of reactants and solids.

These three avenues for transition state tuning are, in principle, complementary, such that it is possible to use more than one or even all at one time. It is likely that there are some systems where more than one effect is present without being presently appreciated. For example, it took some years to fully understand the complex and *dynamic* reaction mechanism in

https://doi.org/10.1021/acs.jpcc.3c02470
J. Phys. Chem. C 2023, 127, 13451−13465

DeNOx over copper sites in zeolites.[126,127] Even today, our community is finding new reactions and new details on old reactions for systems that have been studied for decades. Elucidating and designing complex "active sites" requires some combination of (a) careful experimental protocols, (b) chemical kinetic modeling, and (c) electronic structure calculations. In general, finding out the active structure of metal oxide surfaces (particularly under catalytically active conditions) is nontrivial and presents a major challenge when trying to accurately model adsorbed species and reaction pathways. We are at an early stage in understanding the inherent complexities that arise in dynamic as well as solvated environments, and those complications will provide an additional frontier for research for likely at least another 10 years.

The importance of electronic structure calculations cannot be overstated: In previous decades, the elementary step hypotheses were built upon chemical intuition and experience. Today, electronic structure searches for individual transition states are routine and were essential for conclusions in each section of this Perspective. Today, elementary step hypotheses are increasingly accompanied by single state electronic structure calculations to further strengthen arguments. As computational power and methods continue to evolve, we anticipate the further step of electronic structure molecular dynamics simulations also becoming more common. Such molecular dynamics calculations will provide evidence beyond whether a transition state is feasible and provide stronger evidence for which elementary step pathways and configurations are dominant. Spatial kinetic Monte Carlo methods will likely also play an advancing role in the next 10 years, though they are likely to be less widely utilized than electronic structure molecular dynamics.

We believe understanding the complex chemistry and sites will lead to the following key considerations for future progress: (1) Specialized experiments, especially kinetic and spectroscopic experiments, may need to be consciously designed for mechanistic understanding. (2) Electronic structure calculations (presently represented by density functional theory) will play an increasingly integral role in elucidating such complex mechanistic elementary steps, in part because potential pathways can be nonintuitive or even nondiscriminable unless quantitative comparisons are made to theoretical predictions. (3) It will become increasingly important to build databases of information known about such complex elementary steps over solid catalysts—because both humans and machine learning will need plausible predictions for how these elementary steps may manifest over other solids, and in other environments, and such predictions will not be possible in a general manner unless vast and sophisticated databases are built.

Our *hypotheses* about elementary steps for organic reactions on surfaces are rapidly being supplanted by *knowledge* of the feasible and operative elementary steps for organic reactions on surfaces. We anticipate this trend to continue.

AUTHOR INFORMATION

Corresponding Authors

Victor Fung − *School of Computational Science and Engineering, Georgia Institute of Technology, Atlanta, Georgia 30332, United States;* orcid.org/0000-0002-3347-6983; Email: victorfung@gatech.edu

Michael Janik − *EMS Energy Institute, PSU-DUT Joint Center for Energy Research and Department of Chemical Engineering, The Pennsylvania State University, University Park, Pennsylvania 16802, United States*; Email: mjj13@psu.edu

Steven Crossley − *School of Sustainable Chemical, Biological and Materials Engineering, University of Oklahoma, Norman, Oklahoma 73019, United States;* orcid.org/0000-0002-1017-9839; Email: stevencrossley@ou.edu

Ya-Huei Cathy Chin − *Department of Chemical Engineering and Applied Chemistry, University of Toronto, Toronto M5S 3E5, Canada;* orcid.org/0000-0003-4388-0389; Email: cathy.chin@utoronto.ca

Aditya Savara − *Chemical Sciences Division, Oak Ridge National Laboratory, Oak Ridge, Tennessee 37831-6201, United States;* orcid.org/0000-0002-1937-2571; Email: savaraa@ornl.gov

Complete contact information is available at: https://pubs.acs.org/10.1021/acs.jpcc.3c02470

Author Contributions

V. Fung was the primary author of the latter portion of the section titled "Alkane C−H Bond breaking Reactions" and contributed to the sections "Electronic Structure Considerations & Descriptors" and "Metal Oxides as Lewis Acids/Bases and Atom Abstractors". M. Janik was the primary author of the later portion of the section "Alkane C−H Bond breaking Reactions" and the primary author of the sections "Electronic Structure Considerations and Descriptors" and "Metal Oxides as Lewis Acids/Bases and Atom Abstractors". Y.-H.C. Chin was the primary author of the subsections titled "Dehydration of Alcohols over Confined Acid Sites" and "C−C Bond Formation with Aldehyde Reactants/Intermediates over Confined Acid Sites". S. Crossley was the primary author of the subsections titled "Carboxylic Acids" (on coupling) and "Conversion of Carboxylic Acids over Confined Acid Sites". A. Savara led the writing of the manuscript and was the primary author of the Introduction, Summary, the section titled "C−H Bond Breaking in Alcohols and Aldehydes", and the subsection titled "Aldehydes and Ketones" (on coupling), and he contributed to other sections. The drawn chemical structures in Figures 1, 4, 5, 6, 7, and 8 were created by A. Savara. Figures 11 and 12 were created by Y.H.C. Chin.

Notes

The authors declare no competing financial interest.

A review which expands upon this Perspective with more technical detail is planned.

Biographies

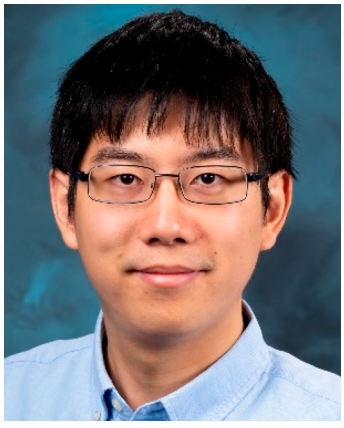

Victor Fung is an Assistant Professor in the School of Computational Science and Engineering at Georgia Tech. He obtained his B.A. in Chemistry from Cornell University (2015) and his Ph.D. in Chemistry from the University of California, Riverside (2019). His research

https://doi.org/10.1021/acs.jpcc.3c02470
J. Phys. Chem. C 2023, 127, 13451−13465

involves the study of surfaces and catalytic properties from first principles.

Michael Janik is a Professor of Chemical Engineering at Pennsylvania State University. His research interests are in the use of computational methods to understand and design materials for alternative energy conversion systems. Research methods emphasize atomistic simulation using quantum chemical methods and kinetic modeling. Dr. Janik received his B.S. from Yale University (1998) and his doctorate from the University of Virginia (2006), both in Chemical Engineering.

Steven Crossley is a Teigen Presidential Professor and Sam A. Wilson Professor in the School of Sustainable Chemical, Biological and Materials Engineering at the University of Oklahoma. He received his B.S. in Chemistry from Oklahoma City University (2004) and a Ph.D. from the University of Oklahoma (2009). His research focuses on elucidating the roles of various surface features on reaction mechanisms in complex reaction environments, focusing primarily on reducible metal oxides and zeolites. His current research interests involve selective conversion of renewable biomass-derived feedstocks, CO_2 free hydrogen generation, and selective conversion of waste polymers.

Ya-Huei (Cathy) Chin is a Professor of Chemical Engineering and Applied Chemistry and Canada Research Chair (Tier II) in Advanced Catalysis for Sustainable Chemistry at the University of Toronto, Canada. Her research focuses on elucidating the molecular events and their kinetic relevance in the activation of hydrocarbons and oxygenates, emphasizing on the mechanistic similarities and differences across the different catalytic systems. She received her B.S. and M.S. degrees (2000) in chemical engineering from University of Oklahoma and her Ph.D. in Chemical Engineering from the University of California, Berkeley (2011).

Aditya "Ashi" Savara is a staff research scientist at Oak Ridge National Laboratory. He received a B.S. in Chemistry from the University of Hawaii (2003) and a Ph.D. in Physical Chemistry from Northwestern University (2008). His research has included work on hydrogen storage, DeNOx catalysis, alkene hydrogenation, and catalytic conversion of oxygenates related to biomass derivatives. Presently, his interests include kinetic Monte Carlo simulations of chemical reactions, ordinary differential based chemical kinetic simulations, and ultrahigh vacuum experiments to elucidate the mechanisms of reactions on surfaces.

■ ACKNOWLEDGMENTS

Work by A. Savara was sponsored by the U.S. Department of Energy, Office of Science, Office of Basic Energy Sciences, Chemical Sciences, Geosciences, and Biosciences Division, Catalysis Science program. Work by S. Crossley was supported from NSF grants 2029394 for selective conversion in confinement discussed in section VIII and 1653935 for the discussion pertaining to deoxygenation over reducible oxides in section VII. Work by M. Janik was supported from NSF grant 2152412.

https://doi.org/10.1021/acs.jpcc.3c02470
J. Phys. Chem. C 2023, 127, 13451−13465

REFERENCES

(1) Miller, J. H.; Bui, L.; Bhan, A. Pathways, Mechanisms, and Kinetics: A Strategy to Examine Byproduct Selectivity in Partial Oxidation Catalytic Transformations on Reducible Oxides. *React. Chem. Eng.* **2019**, *4*, 784−805.

(2) Kuhlenbeck, H.; Shaikhutdinov, S.; Freund, H.-J. Well-Ordered Transition Metal Oxide Layers in Model Catalysis − a Series of Case Studies. *Chem. Rev.* **2013**, *113*, 3986−4034.

(3) McFarland, E. W.; Metiu, H. Catalysis by Doped Oxides. *Chem. Rev.* **2013**, *113*, 4391−4427.

(4) Mullins, D. R. The Surface Chemistry of Cerium Oxide. *Surf. Sci. Rep.* **2015**, *70*, 42−85.

(5) Vohs, J. M. Site Requirements for the Adsorption and Reaction of Oxygenates on Metal Oxide Surfaces. *Chem. Rev.* **2013**, *113*, 4136−4163.

(6) Wang, L.; Maxisch, T.; Ceder, G. Oxidation Energies of Transition Metal Oxides within the $\Mathrm{Gga}+\Mathrm{U}$ Framework. *Phys. Rev. B* **2006**, *73*, 195107.

(7) Weaver, J. F. Surface Chemistry of Late Transition Metal Oxides. *Chem. Rev.* **2013**, *113*, 4164−4215.

(8) Zhuang, G.; Chen, Y.; Zhuang, Z.; Yu, Y.; Yu, J. Oxygen Vacancies in Metal Oxides: Recent Progress Towards Advanced Catalyst Design. *Science China Materials* **2020**, *63*, 2089−2118.

(9) Diebold, U. The Surface Science of Titanium Dioxide. *Surf. Sci. Rep.* **2003**, *48*, 53−229.

(10) Barteau, M. A. Organic Reactions at Well-Defined Oxide Surfaces. *Chem. Rev.* **1996**, *96*, 1413−1430.

(11) Idriss, H.; Barteau, M. A. Active Sites on Oxides: From Single Crystals to Catalysts. *Advances in Catalysis*; Elsevier: 2000; Vol. *45*, pp 261−331.

(12) Goulas, K. A.; Mironenko, A. V.; Jenness, G. R.; Mazal, T.; Vlachos, D. G. Fundamentals of C−O Bond Activation on Metal Oxide Catalysts. *Nature Catalysis* **2019**, *2*, 269−276.

(13) Kostetskyy, P.; Mpourmpakis, G. Structure-Activity Relationships in the Production of Olefins from Alcohols and Ethers: A First-Principles Theoretical Study. *Catal. Sci. Technol.* **2015**, *5*, 4547−4555.

(14) Kostetskyy, P.; Nolan, C. M.; Dixit, M.; Mpourmpakis, G. Understanding Alkane Dehydrogenation through Alcohol Dehydration on Γ-Al2o3. *Ind. Eng. Chem. Res.* **2018**, *57*, 16657−16663.

(15) Latimer, A. A.; Aljama, H.; Kakekhani, A.; Yoo, J. S.; Kulkarni, A.; Tsai, C.; Garcia-Melchor, M.; Abild-Pedersen, F.; Nørskov, J. K. Mechanistic Insights into Heterogeneous Methane Activation. *Phys. Chem. Chem. Phys.* **2017**, *19*, 3575−3581.

(16) Latimer, A. A.; Kakekhani, A.; Kulkarni, A. R.; Nørskov, J. K. Direct Methane to Methanol: The Selectivity−Conversion Limit and Design Strategies. *ACS Catal.* **2018**, *8*, 6894−6907.

(17) Latimer, A. A.; Kulkarni, A. R.; Aljama, H.; Montoya, J. H.; Yoo, J. S.; Tsai, C.; Abild-Pedersen, F.; Studt, F.; Nørskov, J. K. Understanding Trends in C−H Bond Activation in Heterogeneous Catalysis. *Nat. Mater.* **2017**, *16*, 225−229.

(18) Jackson, S. D.; Hargreaves, J. S. *Metal Oxide Catalysis*; John Wiley & Sons: 2008; Vol. *1*.

(19) Capdevila-Cortada, M.; López, N. Descriptor Analysis in Methanol Conversion on Doped Ceo2(111): Guidelines for Selectivity Tuning. *ACS Catal.* **2015**, *5*, 6473−6480.

(20) Sutton, J. E.; Danielson, T.; Beste, A.; Savara, A. Below-Room-Temperature C−H Bond Breaking on an Inexpensive Metal Oxide: Methanol to Formaldehyde on Ceo2(111). *J. Phys. Chem. Lett.* **2017**, *8*, 5810−5814.

(21) Fung, V.; Tao, F.; Jiang, D.-e. Trends of Alkane Activation on Doped Cobalt (Ii, Iii) Oxide from First Principles. *ChemCatChem.* **2018**, *10*, 244−249.

(22) Zhao, Z.-J.; Liu, S.; Zha, S.; Cheng, D.; Studt, F.; Henkelman, G.; Gong, J. Theory-Guided Design of Catalytic Materials Using Scaling Relationships and Reactivity Descriptors. *Nature Reviews Materials* **2019**, *4*, 792−804.

(23) Abdelgaid, M.; Mpourmpakis, G. Structure−Activity Relationships in Lewis Acid−Base Heterogeneous Catalysis. *ACS Catal.* **2022**, *12*, 4268−4289.

(24) Kumar, G.; Lau, S. L. J.; Krcha, M. D.; Janik, M. J. Correlation of Methane Activation and Oxide Catalyst Reducibility and Its Implications for Oxidative Coupling. *ACS Catal.* **2016**, *6*, 1812−1821.

(25) Zhou, C.; Hu, P.; Wang, H. Resolving the Two-Track Scaling Trend for Adsorbates on Rutile-Type Metal Oxides: New Descriptors for Adsorption Energies. *J. Phys. Chem. C* **2021**, *125*, 23162−23168.

(26) Xu, J.; Cao, X.-M.; Hu, P. Improved Prediction for the Methane Activation Mechanism on Rutile Metal Oxides by a Machine Learning Model with Geometrical Descriptors. *J. Phys. Chem. C* **2019**, *123*, 28802−28810.

(27) Jenness, G. R.; Christiansen, M. A.; Caratzoulas, S.; Vlachos, D. G.; Gorte, R. J. Site-Dependent Lewis Acidity of Γ-Al2o3 and Its Impact on Ethanol Dehydration and Etherification. *J. Phys. Chem. C* **2014**, *118*, 12899−12907.

(28) Campbell, C. T.; Sellers, J. R. V. Anchored Metal Nanoparticles: Effects of Support and Size on Their Energy, Sintering Resistance and Reactivity. *Faraday Discuss.* **2013**, *162*, 9−30.

(29) Getsoian, A. B.; Zhai, Z.; Bell, A. T. Band-Gap Energy as a Descriptor of Catalytic Activity for Propene Oxidation over Mixed Metal Oxide Catalysts. *J. Am. Chem. Soc.* **2014**, *136*, 13684−13697.

(30) Fung, V.; Tao, F. F.; Jiang, D.-e. General Structure−Reactivity Relationship for Oxygen on Transition-Metal Oxides. *J. Phys. Chem. Lett.* **2017**, *8*, 2206−2211.

(31) Zhou, C.; Zhang, B.; Hu, P.; Wang, H. An Effective Structural Descriptor to Quantify the Reactivity of Lattice Oxygen in Ceo2 Subnano-Clusters. *Phys. Chem. Chem. Phys.* **2020**, *22*, 1721−1726.

(32) Ouyang, R.; Curtarolo, S.; Ahmetcik, E.; Scheffler, M.; Ghiringhelli, L. M. Sisso: A Compressed-Sensing Method for Identifying the Best Low-Dimensional Descriptor in an Immensity of Offered Candidates. *Physical Review Materials* **2018**, *2*, 083802.

(33) Ouyang, R.; Ahmetcik, E.; Carbogno, C.; Scheffler, M.; Ghiringhelli, L. M. Simultaneous Learning of Several Materials Properties from Incomplete Databases with Multi-Task Sisso. *Journal of Physics: Materials* **2019**, *2*, 024002.

(34) Campbell, C. T. Energies of Adsorbed Catalytic Intermediates on Transition Metal Surfaces: Calorimetric Measurements and Benchmarks for Theory. *Acc. Chem. Res.* **2019**, *52*, 984−993.

(35) Campbell, C. T.; Sellers, J. R. V. Enthalpies and Entropies of Adsorption on Well-Defined Oxide Surfaces: Experimental Measurements. *Chem. Rev.* **2013**, *113*, 4106−4135.

(36) Wu, Z.; Li, M.; Overbury, S. H. On the Structure Dependence of CO Oxidation over Ceo2 Nanocrystals with Well-Defined Surface Planes. *J. Catal.* **2012**, *285*, 61−73.

(37) You, R.; Li, Z.; Zeng, H.; Huang, W. A Flow-Pulse Adsorption-Microcalorimetry System for Studies of Adsorption Processes on Powder Catalysts. *Rev. Sci. Instrum.* **2018**, *89*, 064101.

(38) Xia, X.; Naumann d'Alnoncourt, R.; Strunk, J.; Litvinov, S.; Muhler, M. Coverage-Dependent Kinetics and Thermodynamics of Carbon Monoxide Adsorption on a Ternary Copper Catalyst Derived from Static Adsorption Microcalorimetry. *J. Phys. Chem. B* **2006**, *110*, 8409−8415.

(39) Handy, B. E.; Sharma, S. B.; Spiewak, B. E.; Dumesic, J. A. A Tian-Calvet Heat-Flux Microcalorimeter for Measurement of Differential Heats of Adsorption. *Meas. Sci. Technol.* **1993**, *4*, 1350−1356.

(40) Vannice, M. A.; Sen, B.; Chou, P. Modifications Required on a Power-Compensated Differential Scanning Calorimeter to Obtain Heat of Adsorption Measurements. *Rev. Sci. Instrum.* **1987**, *58*, 647−653.

(41) Saha, A. A Simultaneous Volumetric Adsorption−Isothermal Titration Calorimetry Study of Small Molecules on Supported Metallic Nanoparticles. *J. Therm. Anal. Calorim.* **2016**, *124*, 1623−1634.

(42) Spiewak, B. E.; Dumesic, J. A. Microcalorimetric Measurements of Differential Heats of Adsorption on Reactive Catalyst Surfaces. *Thermochim. Acta* **1997**, *290*, 43−53.

(43) Childers, D.; Saha, A.; Schweitzer, N.; Rioux, R. M.; Miller, J. T.; Meyer, R. J. Correlating Heat of Adsorption of CO to Reaction Selectivity: Geometric Effects Vs Electronic Effects in Neopentane Isomerization over Pt and Pd Catalysts. *ACS Catal.* **2013**, *3*, 2487−2496.

https://doi.org/10.1021/acs.jpcc.3c02470
J. Phys. Chem. C 2023, 127, 13451−13465

(44) Strayer, M. E.; Binz, J. M.; Tanase, M.; Kamali Shahri, S. M.; Sharma, R.; Rioux, R. M.; Mallouk, T. E. Interfacial Bonding Stabilizes Rhodium and Rhodium Oxide Nanoparticles on Layered Nb Oxide and Ta Oxide Supports. *J. Am. Chem. Soc.* **2014**, *136*, 5687−5696.
(45) Veghte, R. M. Insights into the Synthetic Mechanisms Behind Ligand-Free Metal Nanoparticle Formation. Ph.D. Master Thesis, The Pennsylvania State University, 2016.
(46) Jones, A. *Tempature-Programmed Reduction for Solid Materials Characterization*; CRC Press: 1986; Vol. *24*.
(47) Monti, D. A. M.; Baiker, A. Temperature-Programmed Reduction. Parametric Sensitivity and Estimation of Kinetic Parameters. *J. Catal.* **1983**, *83*, 323−335.
(48) Savara, A. Simulation and Fitting of Complex Reaction Network Tpr: The Key Is the Objective Function. *Surf. Sci.* **2016**, *653*, 169−180.
(49) Malet, P.; Caballero, A. The Selection of Experimental Conditions in Temperature-Programmed Reduction Experiments. *J. Chem. Soc., Faraday Trans.* **1988**, *84*, 2369−2375.
(50) Zhang, Y.; Mullins, D. R.; Savara, A. Surface Reactions and Catalytic Activities for Small Alcohols over Lamno3(100) and La0.7sr0.3mno3(100): Dehydrogenation, Dehydration, and Oxidation. *J. Phys. Chem. C* **2020**, *124*, 3650−3663.
(51) Beste, A.; Overbury, S. H. Pathways for Ethanol Dehydrogenation and Dehydration Catalyzed by Ceria (111) and (100) Surfaces. *J. Phys. Chem. C* **2015**, *119*, 2447−2455.
(52) Chin, Y.-H.; Buda, C.; Neurock, M.; Iglesia, E. Consequences of Metal−Oxide Interconversion for C−H Bond Activation During Ch4 Reactions on Pd Catalysts. *J. Am. Chem. Soc.* **2013**, *135*, 15425−15442.
(53) Krcha, M. D.; Mayernick, A. D.; Janik, M. J. Periodic Trends of Oxygen Vacancy Formation and C−H Bond Activation over Transition Metal-Doped Ceo2 (111) Surfaces. *J. Catal.* **2012**, *293*, 103−115.
(54) Colussi, S.; Gayen, A.; Farnesi Camellone, M.; Boaro, M.; Llorca, J.; Fabris, S.; Trovarelli, A. Nanofaceted Pd−O Sites in Pd−Ce Surface Superstructures: Enhanced Activity in Catalytic Combustion of Methane. *Angew. Chem., Int. Ed.* **2009**, *48*, 8481−8484.
(55) Senftle, T. P.; van Duin, A. C. T.; Janik, M. J. Role of Site Stability in Methane Activation on Pdxce1−Xoδ Surfaces. *ACS Catal.* **2015**, *5*, 6187−6199.
(56) Krcha, M. D.; Janik, M. J. Challenges in the Use of Density Functional Theory to Examine Catalysis by M-Doped Ceria Surfaces. *Int. J. Quantum Chem.* **2014**, *114*, 8−13.
(57) Krcha, M. D.; Janik, M. J. Examination of Oxygen Vacancy Formation in Mn-Doped Ceo2 (111) Using Dft+U and the Hybrid Functional Hse06. *Langmuir* **2013**, *29*, 10120−10131.
(58) Savara, A.; Walker, E. A. Chekipeuq Intro 1: Bayesian Parameter Estimation Considering Uncertainty or Error from Both Experiments and Theory. *ChemCatChem.* **2020**, *12*, 5385−5400.
(59) Walker, E. A.; Ravisankar, K.; Savara, A. Chekipeuq Intro 2: Harnessing Uncertainties from Data Sets, Bayesian Design of Experiments in Chemical Kinetics. *ChemCatChem.* **2020**, *12*, 5401−5410.
(60) Matera, S.; Schneider, W. F.; Heyden, A.; Savara, A. Progress in Accurate Chemical Kinetic Modeling, Simulations, and Parameter Estimation for Heterogeneous Catalysis. *ACS Catal.* **2019**, *9*, 6624−6647.
(61) Hellman, A.; Resta, A.; Martin, N. M.; Gustafson, J.; Trinchero, A.; Carlsson, P. A.; Balmes, O.; Felici, R.; van Rijn, R.; Frenken, J. W. M.; et al. The Active Phase of Palladium During Methane Oxidation. *J. Phys. Chem. Lett.* **2012**, *3*, 678−682.
(62) Antony, A.; Asthagiri, A.; Weaver, J. F. Pathways and Kinetics of Methane and Ethane C−H Bond Cleavage on Pdo(101). *J. Chem. Phys.* **2013**, *139*, 104702.
(63) Pérez-Ramírez, J.; López, N. Strategies to Break Linear Scaling Relationships. *Nature Catalysis* **2019**, *2*, 971−976.
(64) Choi, C.; Yoon, S.; Jung, Y. Shifting the Scaling Relations of Single-Atom Catalysts for Facile Methane Activation by Tuning the Coordination Number. *Chemical Science* **2021**, *12*, 3551−3557.
(65) Szécsényi, Á.; Khramenkova, E.; Chernyshov, I. Y.; Li, G.; Gascon, J.; Pidko, E. A. Breaking Linear Scaling Relationships with Secondary Interactions in Confined Space: A Case Study of Methane Oxidation by Fe/Zsm-5 Zeolite. *ACS Catal.* **2019**, *9*, 9276−9284.
(66) Fung, V.; Polo-Garzon, F.; Wu, Z.; Jiang, D.-e. Exploring Perovskites for Methane Activation from First Principles. *Catal. Sci. Technol.* **2018**, *8*, 702−709.
(67) Sun, G.; Zhao, Z.-J.; Mu, R.; Zha, S.; Li, L.; Chen, S.; Zang, K.; Luo, J.; Li, Z.; Purdy, S. C.; et al. Breaking the Scaling Relationship Via Thermally Stable Pt/Cu Single Atom Alloys for Catalytic Dehydrogenation. *Nat. Commun.* **2018**, *9*, 4454.
(68) Liu, Z.; Huang, E.; Orozco, I.; Liao, W.; Palomino, R. M.; Rui, N.; Duchoň, T.; Nemšák, S.; Grinter, D. C.; Mahapatra, M.; et al. Water-Promoted Interfacial Pathways in Methane Oxidation to Methanol on a Ceo < Sub > 2</Sub>-Cu < Sub > 2</Sub > O Catalyst. *Science* **2020**, *368*, 513−517.
(69) Shinohara, Y.; Nakajima, T.; Suzuki, S. A Theoretical Study of the Dehydration and the Dehydrogenation Processes of Alcohols on Metal Oxides Using Mopac. *Journal of Molecular Structure: THEOCHEM* **1999**, *460*, 231−244.
(70) Roy, S.; Mpourmpakis, G.; Hong, D.-Y.; Vlachos, D. G.; Bhan, A.; Gorte, R. J. Mechanistic Study of Alcohol Dehydration on Γ-Al2o3. *ACS Catal.* **2012**, *2*, 1846−1853.
(71) Kostestkyy, P.; Yu, J.; Gorte, R. J.; Mpourmpakis, G. Structure−Activity Relationships on Metal-Oxides: Alcohol Dehydration. *Catal. Sci. Technol.* **2014**, *4*, 3861−3869.
(72) Badlani, M.; Wachs, I. E. Methanol: A "Smart" Chemical Probe Molecule. *Catal. Lett.* **2001**, *75*, 137−149.
(73) Chong, S.; Griffiths, T.; Idriss, H. Ethanol Reactions over the Uo2 (111) Single Crystal: Effect of the Madelung Potential on the Reaction Selectivity. *Surf. Sci.* **2000**, *444*, 187−198.
(74) Zabilska, A.; Clark, A. H.; Moskowitz, B. M.; Wachs, I. E.; Kakiuchi, Y.; Copéret, C.; Nachtegaal, M.; Krocher, O.; Safonova, O. V. Redox Dynamics of Active Vo X Sites Promoted by Tio X During Oxidative Dehydrogenation of Ethanol Detected by Operando Quick Xas. *Jacs Au* **2022**, *2*, 762−776.
(75) Davis, B. Alcohol Conversion Selectivity as a Measure of the Base Strength of Metal Oxide Catalysts. *Studies in Surface Science and Catalysis*; Elsevier: 1985; Vol. *21*, pp 309−318.
(76) Sato, S.; Sato, F.; Gotoh, H.; Yamada, Y. Selective Dehydration of Alkanediols into Unsaturated Alcohols over Rare Earth Oxide Catalysts. *ACS Catal.* **2013**, *3*, 721−734.
(77) Niiyama, H.; Echigoya, E. Dehydration and Dehydrogenation of Alcohols over Acid-Base Bifunctional Catalysts. *Bull. Chem. Soc. Jpn.* **1971**, *44*, 1739−1742.
(78) Rousseau, R.; Dixon, D. A.; Kay, B. D.; Dohnálek, Z. Dehydration, Dehydrogenation, and Condensation of Alcohols on Supported Oxide Catalysts Based on Cyclic (Wo3)3 and (Moo3)3 Clusters. *Chem. Soc. Rev.* **2014**, *43*, 7664−7680.
(79) Bond, G. C.; Flamerz, S.; Shukri, R. Structure and Reactivity of Transition-Metal Oxide Monolayers. *Faraday discussions of the Chemical Society* **1989**, *87*, 65−77.
(80) Burcham, L. J.; Briand, L. E.; Wachs, I. E. Quantification of Active Sites for the Determination of Methanol Oxidation Turn-over Frequencies Using Methanol Chemisorption and in Situ Infrared Techniques. 1. Supported Metal Oxide Catalysts. *Langmuir* **2001**, *17*, 6164−6174.
(81) Zhang, W.; Desikan, A.; Oyama, S. T. Effect of Support in Ethanol Oxidation on Molybdenum Oxide. *J. Phys. Chem.* **1995**, *99*, 14468−14476.
(82) Chen, B.; Xiong, C.; Jiang, D.-e.; Savara, A. Ethanol Conversion over La0.7sr0.3mno3−X(100): Autocatalysis, Adjacent O-Vacancies, Disproportionation, and Dehydrogenation. *ACS Catal.* **2020**, *10*, 12920−12931.
(83) Nolte, M. W.; Shanks, B. H. A Perspective on Catalytic Strategies for Deoxygenation in Biomass Pyrolysis. *Energy Technology* **2017**, *5*, 7−18.
(84) Li, F.; Wang, B.; Chen, X.; Fan, H.; Yang, X.; Guo, Q. Low-Temperature Aldol Condensation of Aldehydes on R-Tio2(100)-(1 × 1): Exceptional Selectivity for A,B-Unsaturated Enal Production. *J. Phys. Chem. Lett.* **2021**, *12*, 1708−1717.

https://doi.org/10.1021/acs.jpcc.3c02470
J. Phys. Chem. C 2023, 127, 13451−13465

(85) Kozlowski, J. T.; Davis, R. J. Heterogeneous Catalysts for the Guerbet Coupling of Alcohols. *ACS Catal.* **2013**, *3*, 1588−1600.
(86) Taifan, W. E.; Bučko, T.; Baltrusaitis, J. Catalytic Conversion of Ethanol to 1,3-Butadiene on Mgo: A Comprehensive Mechanism Elucidation Using Dft Calculations. *J. Catal.* **2017**, *346*, 78−91.
(87) Zhao, C.; Watt, C.; Kent, P. R.; Overbury, S. H.; Mullins, D. R.; Calaza, F. C.; Savara, A.; Xu, Y. Coupling of Acetaldehyde to Crotonaldehyde on Ceo_2−X(111): Bifunctional Mechanism and Role of Oxygen Vacancies. *J. Phys. Chem. C* **2019**, *123*, 8273−8286.
(88) Palagin, D.; Sushkevich, V. L.; Ivanova, I. I. C−C Coupling Catalyzed by Zeolites: Is Enolization the Only Possible Pathway for Aldol Condensation? *J. Phys. Chem. C* **2016**, *120*, 23566−23575.
(89) Bhasker-Ranganath, S.; Rahman, M. S.; Zhao, C.; Calaza, F.; Wu, Z.; Xu, Y. Elucidating the Mechanism of Ambient-Temperature Aldol Condensation of Acetaldehyde on Ceria. *ACS Catal.* **2021**, *11*, 8621−8634.
(90) Pacchioni, G. Ketonization of Carboxylic Acids in Biomass Conversion over Tio2 and Zro2 Surfaces: A Dft Perspective. *ACS Catal.* **2014**, *4*, 2874−2888.
(91) Pham, T. N.; Sooknoi, T.; Crossley, S. P.; Resasco, D. E. Ketonization of Carboxylic Acids: Mechanisms, Catalysts, and Implications for Biomass Conversion. *ACS Catal.* **2013**, *3*, 2456−2473.
(92) Barteau, M. A. New Catalysis from Metal Oxide Surface Science. *Studies in Surface Science and Catalysis*; Elsevier: 2000; Vol. *130*, pp 105−114.
(93) Pestman, R.; Koster, R. M.; Pieterse, J. A. Z.; Ponec, V. Reactions of Carboxylic Acids on Oxides. 1. Selective Hydrogenation of Acetic Acid to Acetaldehyde. *J. Catal.* **1997**, *168*, 255−264.
(94) Pestman, R.; Vanduijne, A.; Pieterse, J. A. Z.; Ponec, V. The Formation of Ketones and Aldehydes from Carboxylic-Acids, Structure-Activity Relationship for 2 Competitive Reactions. *J. Mol. Catal. a-Chem.* **1995**, *103*, 175−180.
(95) Martinez, R.; Huff, M. C.; Barteau, M. A. Ketonization of Acetic Acid on Titania-Functionalized Silica Monoliths. *J. Catal.* **2004**, *222*, 404−409.
(96) Tosoni, S.; Pacchioni, G. Acetic Acid Ketonization on Tetragonal Zirconia: Role of Surface Reduction. *J. Catal.* **2016**, *344*, 465−473.
(97) Pham, T. N.; Shi, D.; Sooknoi, T.; Resasco, D. E. Aqueous-Phase Ketonization of Acetic Acid over Ru/Tio2/Carbon Catalysts. *J. Catal.* **2012**, *295*, 169−178.
(98) Ignatchenko, A. V. Multiscale Approach for the Optimization of Ketones Production from Carboxylic Acids by the Decarboxylative Ketonization Reaction. *Catal. Today* **2019**, *338*, 3−17.
(99) Wang, S.; Iglesia, E. Experimental and Theoretical Assessment of the Mechanism and Site Requirements for Ketonization of Carboxylic Acids on Oxides. *J. Catal.* **2017**, *345*, 183−206.
(100) Pham, T. N.; Shi, D.; Resasco, D. E. Kinetics and Mechanism of Ketonization of Acetic Acid on Ru/Tio2 Catalyst. *Top. Catal.* **2014**, *57*, 706−714.
(101) Zhu, J.; Vuong, V. Q.; Sumpter, B. G.; Irle, S. Artificial Neural Network Correction for Density-Functional Tight-Binding Molecular Dynamics Simulations. *MRS Commun.* **2019**, *9*, 867−873.
(102) Hutama, A. S.; Marlina, L. A.; Chou, C.-P.; Irle, S.; Hofer, T. S. Development of Density-Functional Tight-Binding Parameters for the Molecular Dynamics Simulation of Zirconia, Yttria, and Yttria-Stabilized Zirconia. *ACS Omega* **2021**, *6*, 20530−20548.
(103) Pineda, M.; Stamatakis, M. Kinetic Monte Carlo Simulations for Heterogeneous Catalysis: Fundamentals, Current Status, and Challenges. *J. Chem. Phys.* **2022**, *156*, 120902.
(104) Fečík, M.; Plessow, P. N.; Studt, F. Simple Scheme to Predict Transition-State Energies of Dehydration Reactions in Zeolites with Relevance to Biomass Conversion. *J. Phys. Chem. C* **2018**, *122*, 23062−23067.
(105) John, M.; Alexopoulos, K.; Reyniers, M.-F.; Marin, G. B. Mechanistic Insights into the Formation of Butene Isomers from 1-Butanol in H-Zsm-5: Dft Based Microkinetic Modelling. *Catal. Sci. Technol.* **2017**, *7*, 1055−1072.
(106) Nguyen, C. M.; Reyniers, M. F.; Marin, G. B. Theoretical Study of the Adsorption of the Butanol Isomers in H-Zsm-5. *J. Phys. Chem. C* **2011**, *115*, 8658−8669.
(107) Kunz, L. Y.; Bu, L.; Knott, B. C.; Liu, C.; Nimlos, M. R.; Assary, R. S.; Curtiss, L. A.; Robichaud, D. J.; Kim, S. Theoretical Determination of Size Effects in Zeolite-Catalyzed Alcohol Dehydration. *Catalysts* **2019**, *9*, 700.
(108) Wang, S.; Iglesia, E. Catalytic Diversity Conferred by Confinement of Protons within Porous Aluminosilicates in Prins Condensation Reactions. *J. Catal.* **2017**, *352*, 415−435.
(109) Hunter, E. P. L.; Lias, S. G. *Evaluated Gas Phase Basicities and Proton Affinities of Molecules: An Update* **1998**, *27*, 413−656.
(110) Wróblewski, T.; Ziemczonek, L.; Szerement, K.; Karwasz, G. P. Proton Affinities of Simple Organic Compounds. *Czech. J. Phys.* **2006**, *56*, B1110−B1115.
(111) Lin, F.; Yang, Y.; Chin, Y.-H. Kinetic Requirements of Aldehyde Transfer Hydrogenation Catalyzed by Microporous Solid Brønsted Acid Catalysts. *ACS Catal.* **2017**, *7*, 6909−6914.
(112) Bajorek, J. J. S.; Battaglia, R.; Pratt, G.; Sutherland, J. K. A Modified Prins Reaction Applicable to Conjugated Dienes. *J. Chem. Soc., Perkin Trans. 1* **1974**, 1243−1245.
(113) Lin, F.; Chin, Y.-H. Mechanism of Intra- and Inter-Molecular CC Bond Formation of Propanal on Brønsted Acid Sites Contained within MFI Zeolites. *J. Catal.* **2014**, *311*, 244−256.
(114) Lin, F.; Chin, Y.-H. C. Catalytic Pathways and Kinetic Requirements for Alkanal Deoxygenation on Solid Tungstosilicic Acid Clusters. *ACS Catal.* **2016**, *6*, 6634−6650.
(115) Lin, F.; Chin, Y.-H. Alkanal Transfer Hydrogenation Catalyzed by Solid Brønsted Acid Sites. *The. J. Catal.* **2016**, *341*, 136−148.
(116) Lin, F.; Zhang, J.; Liu, D.; Chin, Y.-H. Cascade Reactions in Tunable Lamellar Micro- and Mesopores for C═C Bond Coupling and Hydrocarbon. *Synthesis.* **2018**, *57*, 12886−12890.
(117) Yang, Y.; Lin, F.; Tran, H.; Chin, Y.-H. Butanal Condensation Chemistry Catalyzed by Brønsted Acid Sites on Polyoxometalate Clusters. *ChemCatChem.* **2017**, *9*, 287−299.
(118) Bejblova, M.; Prochazkova, D.; Čejka, J. Acylation Reactions over Zeolites and Mesoporous Catalysts. *ChemSusChem: Chemistry & Sustainability Energy & Materials* **2009**, *2*, 486−499.
(119) Gumidyala, A.; Sooknoi, T.; Crossley, S. Selective Ketonization of Acetic Acid over Hzsm-5: The Importance of Acyl Species and the Influence of Water. *J. Catal.* **2016**, *340*, 76−84.
(120) Corma, A.; JoséCliment, M.; García, H.; Primo, J. Design of Synthetic Zeolites as Catalysts in Organic Reactions: Acylation of Anisole by Acyl Chlorides or Carboxylic Acids over Acid Zeolites. *Applied catalysis* **1989**, *49*, 109−123.
(121) Gumidyala, A.; Wang, B.; Crossley, S. Direct Carbon-Carbon Coupling of Furanics with Acetic Acid over Brønsted Zeolites. *Science advances* **2016**, *2*, e1601072.
(122) Chau, H. K.; Resasco, D. E.; Do, P.; Crossley, S. P. Acylation of m-cresol with acetic acid supported by in-situ ester formation on H-ZSM-5 zeolites. *Journal of Catalysis* **2022**, *406*, 48−55.
(123) Chen, T.-H.; Vlachos, D. G.; Caratzoulas, S. Brønsted Acid Catalysis of the Direct Acylation of 2-Methylfuran by Acetic Acid. Theoretical Insights into the Role of Brønsted Acidity and Confinement. *ACS Catal.* **2021**, *11*, 9916−9925.
(124) Koehle, M.; Zhang, Z.; Goulas, K. A.; Caratzoulas, S.; Vlachos, D. G.; Lobo, R. F. Acylation of Methylfuran with Brønsted and Lewis Acid Zeolites. *Applied Catalysis A: General* **2018**, *564*, 90−101.
(125) Crossley, S. P.; Resasco, D. E.; Haller, G. L. Clarifying the Multiple Roles of Confinement in Zeolites: From Stabilization of Transition States to Modification of Internal Diffusion Rates. *J. Catal.* **2019**, *372*, 382−387.
(126) Paolucci, C.; Khurana, I.; Parekh, A. A.; Li, S.; Shih, A. J.; Li, H.; Di Iorio, J. R.; Albarracin-Caballero, J. D.; Yezerets, A.; Miller, J. T.; et al. Dynamic Multinuclear Sites Formed by Mobilized Copper Ions in NO_x Selective Catalytic Reduction. *Science* **2017**, *357*, 898−903.
(127) Paolucci, C.; Di Iorio, J. R.; Schneider, W. F.; Gounder, R. Solvation and Mobilization of Copper Active Sites in Zeolites by

https://doi.org/10.1021/acs.jpcc.3c02470
J. Phys. Chem. C 2023, 127, 13451−13465

Ammonia: Consequences for the Catalytic Reduction of Nitrogen Oxides. *Acc. Chem. Res.* **2020**, *53*, 1881−1892.

https://doi.org/10.1021/acs.jpcc.3c02470
J. Phys. Chem. C 2023, 127, 13451−13465